

A reference free ultrasonic phased array to identify surface cracks in welded steel pipes based on transmissibility

Yun-Lai Zhou^a, Xudong Qian^{a,*}, Alistair Birnie^{b,c}, Xiao-Ling Zhao^d

^a Centre for Offshore Research and Engineering, Department of Civil and Environmental Engineering, National University of Singapore, Singapore 117576

^b Centre for Offshore Research and Engineering, Department of Mechanical Engineering, National University of Singapore, Singapore 117576

^c Denmore Technologies Ltd., 6 Lochside Road, Bridge of Don, Aberdeen, Scotland, United Kingdom

^d Department of Civil Engineering, Monash University, Clayton, VIC 3800, Australia



ARTICLE INFO

Keywords:

Surface crack
Crack sizing
Transmissibility
Ultrasonic phased array testing
Welded pipes

ABSTRACT

This study aims to enhance the precision of ultrasonic phased array (UPA) testing in detecting and sizing the circumferential surface cracks near the girth welds of the steel pipes, via implementing, for the first time, the transmissibility analysis on the ultrasonic scan data. The transmissibility-based approach detects the presence of cracks or crack-like flaws, solely from the relative magnitude of the A-scan data in intact materials and in materials with a crack, and hence removes the requirement for a reference block, but retains the material characteristics. This study also proposes a new approach to detect cracks by the transmissibility between measured ultrasonic A-scan data at distinct locations. Through a relative movement of the UPA sensor, the crack depths derive from the wave propagation theory. The comparison against conventional UPA tests and measurement from replica-reproduced fracture surfaces, in seven circumferentially welded steel pipes with surface cracks produced by fatigue and fracture tests, verifies the applicability of proposed crack sizing approach. The experimental study also examines the distance threshold from the crack location, within which a reasonable accurate crack sizing remains tractable.

1. Introduction

Steel pipelines with circumferential welds remain as a critical infrastructure in transporting hydrocarbon products in both onshore and offshore environments around the world and has been a research focus during the past few years [1–3]. Integrity management of such welded pipelines requires accurate detection and sizing of the defects, especially near the circumferential girth welds, through a non-destructive testing (NDT) approach. Despite the vast application of welded steel pipeline in the industry, efficient and precise sizing of internal or external cracks in the vicinity of welds remains a challenging task for practicing engineers using the latest available NDT tools [4].

Previous researchers have implemented various approaches in sizing the surface cracks in welded joints, e.g., the alternating current potential difference (ACPD) approach [5–10], the acoustic method [9,11,12], the compliance-based approach for fracture specimens [13–15], eddy current array testing [16,17] and the ultrasonic phased array approach [18–21]. Crack detection and sizing have also become an inseparable effort in the broad structural damage detection research [22] using the physical model based technique [23], the data or

statistical model based approach [24,25], and the model updating based approach [18]. Among these techniques, the ultrasonic phased array (UPA) has found wide applications in welded pipes [26,27], friction stirred welds [28,29] and other structural components [30–34]. However, the practical implementation of the UPA for different materials and environmental conditions faces a critical bottleneck in establishing the reference conditions for a wide range of flaw types and service conditions, through the user calibration to ensure the accuracy and reliability of the UPA detection [35]. Fig. 1 illustrates a typical scenario where both the flaw configurations and the service environment evolve over time and thus remain time-dependent. This leads to significant efforts in establishing the reference blocks required in the UPA test. A number of researchers have developed various approaches to enhance the accuracy of UPA. Wilcox et al. [36] have proposed two algorithms for post-processing the UPA data to obtain the reflector orientation and to distinguish the point-like reflectors from the specular reflectors. Their results indicate that the 1-mm-long slots can be distinguished from the 1-mm diameter circular hole. Guan et al. [37] have developed a post-processing strategy to re-sample non-uniformly distributed UPA points to a uniform volume.

* Corresponding author.

E-mail address: qianxudong@nus.edu.sg (X. Qian).

Nomenclature

A	Amplitude of the emitted ultrasonic wave
C	Defined norm
d	Crack depth
F	Emitting wave function
g	Source function
h	Crack height
k	Constant
P	Number of sensors
Q	Defined norm
R	Received wave at certain location
s	The area of wave propagated
S	Horizontal distance
t	Time domain
T	Transmissibility
ω	Frequency
x	Horizontal coordinates
y	Vertical coordinates

X	Structural response
α	Ultrasonic emitting angle
β	Ultrasonic emitting angle
γ	Phase angle
η	Shape functions
ξ	Attenuation function
ϕ	Field variable
<i>Superscript/ subscript</i>	
d	Value under damaged condition
e	The value for eth element
f	f^{th} field variable
i	i^{th} position
j	j^{th} position
p	p^{th} field variable
u	Value under undamaged condition
v	v^{th} sensor

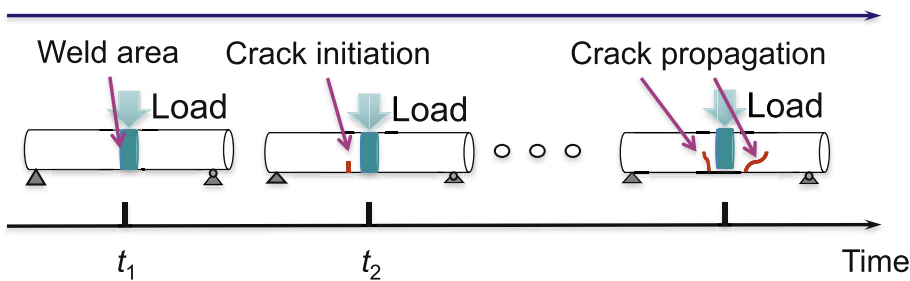
Variations in loadings and environmental conditions

Fig. 1. Evolving crack configuration, loading and environmental conditions with respect to time.

To relinquish the requirement of a reference block, this study proposes a transmissibility-based treatment on the UPA A-scan data. The transmissibility method has observed extensive applications in the structural health monitoring (SHM) for damage detection and damage quantification in the last few decades [22,38–43]. The transmissibility defines the ratio between the structural responses at different locations, e.g., the ratio of a response in a damaged location and that at an intact location measured at the same time. The transmissibility makes redundant of the reference block, which is otherwise mandatory in the UPA test, since 1) the ratio of the responses indicates the occurrence of the damage; and 2) the structural response measured at the same time reflects the evolving crack configurations and service conditions.

This study aims to extend, for the first time, the transmissibility concept to the UPA test, to size cracks near the weld toe of the circumferentially welded circular pipes using the ultrasonic A-scan data. The comparison of the conventional UPA measurement and direct measurement of the crack size through replica-reproduced fracture surface confirms the accuracy of the proposed approach.

The remaining of this paper is organized as follows. Section 2 introduces the background of transmissibility and transmissibility-based crack sizing approach using the ultrasonic test A-scan data. Section 3 discusses the UPA test and physical measurement using replica, and the comparison between these crack sizing approaches. Section 4 presents the experimental program on seven pipe specimens with girth welds. Section 5 discusses the experimental results and validates the proposed transmissibility-based approach. Section 6 summarizes the main conclusions of this study.

2. Transmissibility-enhanced UPA

2.1. Ultrasonic wave based transmissibility

This section aims to provide some theoretical background to extend the transmissibility to the ultrasonic phased array. Since the transmissibility has demonstrated its success in vibration-based data analysis, extension of the transmissibility remains valid if the wave propagation of the ultrasonic phased array follows the same characteristic equation as the vibration analysis.

As discussed in Ref. [44], the wave propagation follows typically the Helmholtz's equation:

$$\nabla^2\phi + k^2\phi = g \quad (1)$$

where ϕ is the field variable, g is the source function, and k is constant (called wavenumber), which denotes the number of waves per 2π units of length.

The functional corresponding to Eq. (1) follows,

$$I(\phi) = \frac{1}{2} \int \int [|\nabla\phi|^2 - k^2\phi^2 + 2\phi g] ds \quad (2)$$

where ds indicates the area of the wave propagated. By defining the field variable and the source function as shape functions over a triangular element, we have,

$$\begin{cases} \phi_e(x, y) = \sum_{i=1}^3 \eta_i \phi_{ei} \\ g_e(x, y) = \sum_{i=1}^3 \eta_i g_{ei} \end{cases} \quad (3)$$

where $\eta_i(x, y)$ represents the shape functions. Using two norms,

$$\begin{cases} C_{ij} = \int \int \nabla \eta_i \cdot \nabla \eta_j ds \\ Q_{ij} = \int \int \nabla \eta_i \cdot \eta_j ds \end{cases} \quad (4)$$

Eq. (2) becomes,

$$I(\phi) = \frac{1}{2} \begin{bmatrix} \phi_f^T \phi_p^T \\ C_{pf} \end{bmatrix} \begin{bmatrix} C_{ff} & C_{fp} \\ C_{pf} & C_{pp} \end{bmatrix} \begin{bmatrix} \phi_f \\ \phi_p \end{bmatrix} - \frac{k^2}{2} \begin{bmatrix} \phi_f^T \phi_p^T \\ Q_{pf} \end{bmatrix} \begin{bmatrix} Q_{ff} & Q_{fp} \\ Q_{pf} & Q_{pp} \end{bmatrix} \begin{bmatrix} \phi_f \\ \phi_p \end{bmatrix} \quad (5)$$

For the functional in Eqs. (2) and (5) to be minimum, we have,

$$\nabla I(\phi) = [C_{ff} \ C_{fp}] \begin{bmatrix} \phi_f \\ \phi_p \end{bmatrix} - k^2 [Q_{ff} \ Q_{fp}] \begin{bmatrix} \phi_f \\ \phi_p \end{bmatrix} = 0 \quad (6)$$

which is a system of linear equations. Assuming all prescribed values to be zero leads to,

$$\nabla I(\phi) = [[C_{ff}] - k^2 [Q_{ff}]] \phi_f = 0 \quad (7)$$

Equation (7) represents a standard eigen-problem [45,46], same as the characteristic function in the vibration analysis [47].

For a structure subjected to a single source ultrasonic wave probe shown in Fig. 2, considering a UPA probe with P (1, 2, 3, ..., P) single wave emitting (and receiving) sensors, the emitting wave at the structural surface has the following form,

$$F_v = A_v \times \sin(\omega_v t + \gamma_v) \quad (8)$$

where $v = 1, 2, 3, \dots, P$. A_v denotes the amplitude of the emitted ultrasonic wave, ω_v refers to the frequency of the emitted wave, and γ_v indicates the phase angle.

The received waves at two arbitrary positions i and j follow,

$$R_i = \xi_{(v,i)} \times \sum_{v=1}^{N_p} F_v = \sum_{v=1}^{N_p} A_v \times \sin(\omega_v t + \gamma_v) \xi_{(v,i)} \quad (9)$$

$$R_j = \xi_{(v,j)} \times \sum_{v=1}^{N_p} F_v = \sum_{v=1}^{N_p} A_v \times \sin(\omega_v t + \gamma_v) \xi_{(v,j)} \quad (10)$$

where $\xi_{(v,j)}$ depicts the attenuation of the wave, which relies on the received wave position, and the material property distribution, i.e. $\xi_{(v,j)} \sim (x, y, v)$.

Recalling the transmissibility definition [38], the transmissibility between point i and a reference point j for a structural system follows,

$$T_{(i,j)} = \frac{X_i}{X_j} \quad (11)$$

where X_i and X_j refer to the structural responses (e.g. strain, displacement, acceleration, etc.) at point i and j , respectively. In this study, X_i and X_j denote the magnitude of the A-scan data measured at each location. The position j may represent either an intact or a damaged location. The transmissibility for the received ultrasonic wave at points i and j thus becomes,

$$T_{(i,j)} = \frac{R_i}{R_j} = \frac{\sum_{v=1}^{N_p} A_v \times \sin(\omega_v t + \gamma_v) \times \xi_{(v,i)}}{\sum_{v=1}^{N_p} A_v \times \sin(\omega_v t + \gamma_v) \times \xi_{(v,j)}} \quad (12)$$

This transmissibility $T_{(i,j)}$ reflects the material characteristics, since the wave frequency, phase, and attenuation coefficient depend on the material property.

For a series of responses measured on N_m nodes, the transmissibility parameter in Eq. (11) expands into a matrix,

$$T_{ij} = \begin{bmatrix} T_{(1,1)} & T_{(1,2)} & \cdots & T_{(1,N_m-1)} & T_{(1,N_m)} \\ T_{(2,1)} & T_{(2,2)} & \cdots & T_{(2,N_m-1)} & T_{(2,N_m)} \\ \vdots & \vdots & T_{(i,j)} & \vdots & \vdots \\ T_{(N_m-1,1)} & T_{(N_m-1,2)} & \cdots & T_{(N_m-1,N_m-1)} & T_{(N_m-1,N_m)} \\ T_{(N_m,1)} & T_{(N_m,2)} & \cdots & T_{(N_m,N_m-1)} & T_{(N_m,N_m)} \end{bmatrix} \quad (13)$$

In Eq. (11), the reference selection remains a challenging but important task. When applied to the A-scan data from the UPA, the reference condition becomes tractable by imposing a threshold on the measured magnitude of the response X_j . Alternatively, a sufficiently large coverage of measurement points in Eq. (13) allows the determination of the intact reference locations, as the transmissibility of the signal from the intact location to a damaged position shows typically a value far below 1.0, while the transmissibility of the intact point over other points should not far exceed 1.0.

2.2. Crack indicator

The crack indicator provides a convenient index in determining the occurrence of cracks. This study utilizes the transmissibility difference as the crack indicator,

$$\Delta T_{(i,j)} = \left| \frac{T_{(i,j)}^d - T_{(i,j)}^u}{T_{(i,j)}^u} \right| \times 100\% \quad (14)$$

where $T_{(i,j)}^d$ denotes the value under a damaged condition, and $T_{(i,j)}^u$ refers to the value under an undamaged condition. For S355 steels at intact conditions, T^u equals approximately 1.0 and the material remains

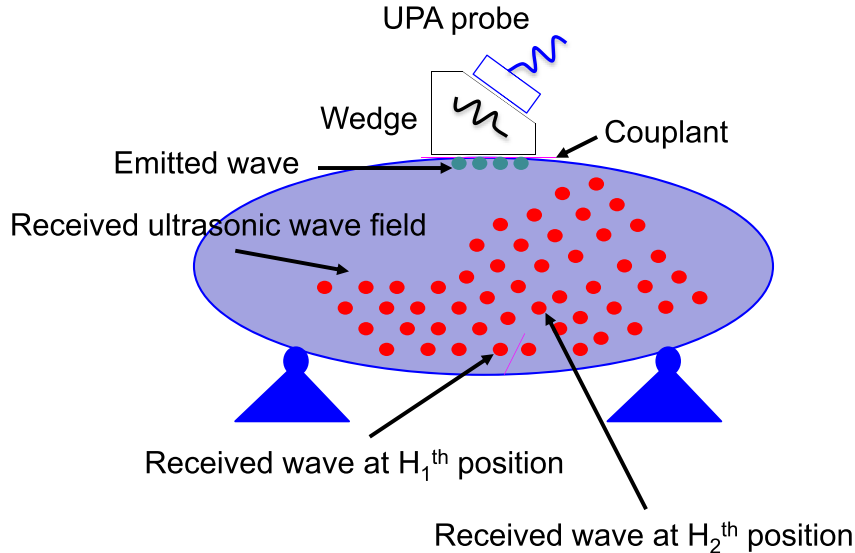


Fig. 2. Transmissibility for UPA tested data.

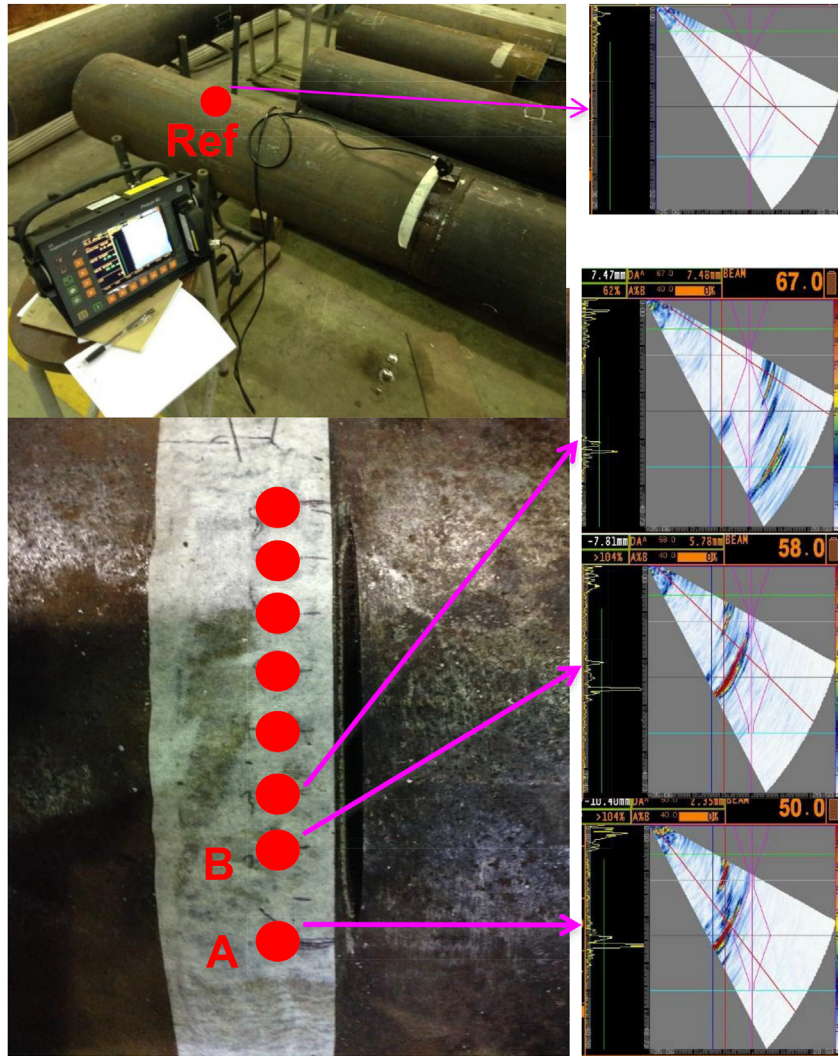


Fig. 3. Illustration of ultrasonic phased array arrangement prepared for subsequent transmissibility treatment.

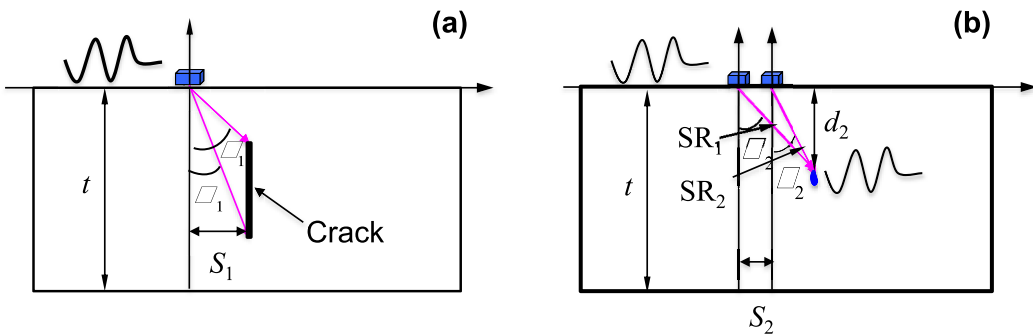


Fig. 4. Crack sizing strategies based on: (a) distance S_1 calculated from material-dependent ultrasonic speed; and (b) material independent relative movement S_2 .

isotropic and homogenous. Equation (14) requires a tolerance to detect the crack occurrence. For the dense materials like S355 steels, a tolerance threshold of 10% is sufficient to pick up the signals reflected by a discontinuity. For porous materials, e.g., the carbon fiber reinforced polymer (CFRP), a detailed investigation is required to quantify the threshold level in order to distinguish the signals reflected by the discontinuity caused by a defect.

2.3. Crack detection and sizing

The transmissibility-based UPA separates into the crack detection and crack sizing stages, as detailed below.

The crack detection stage utilizes the crack indicator in Eq. (14). The UPA A-scan data measured at N_m locations along the specimen, as shown in Fig. 3, leads to the transmissibility matrix in Eq. (13). Based on the crack indicator in Eq. (14), a crack occurs if the magnitude of the crack indicator at a position exceeds a threshold value (10% in this study).

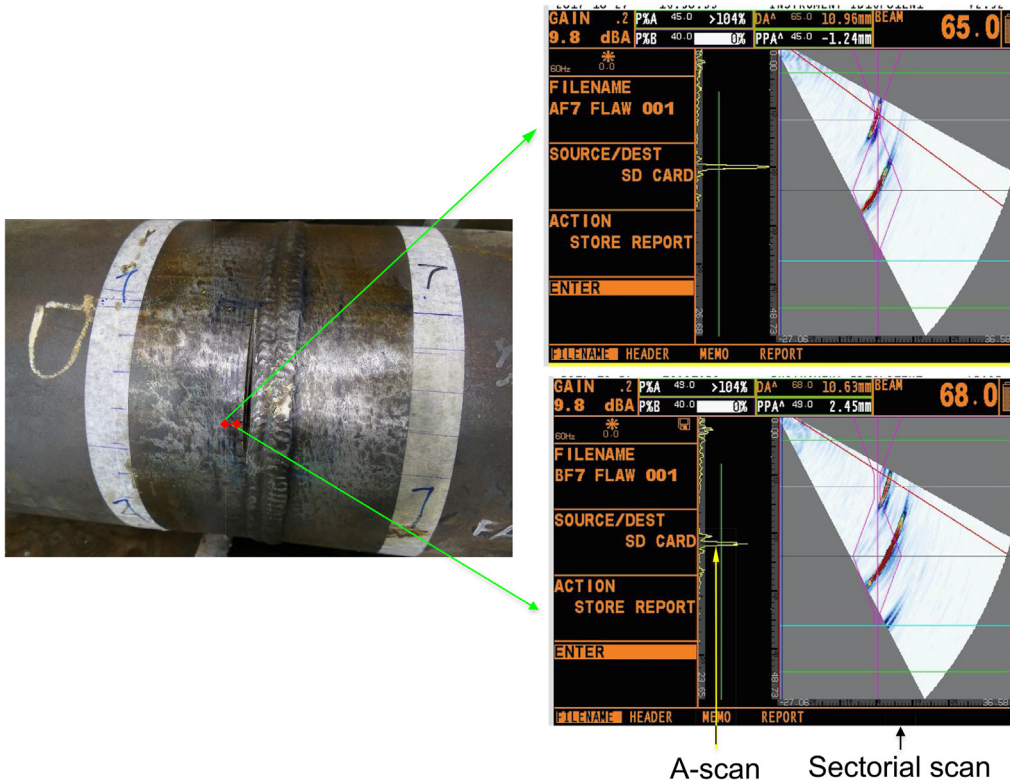


Fig. 5. Typical A-scan and sectorial scan measured from the welded pipes at different locations.

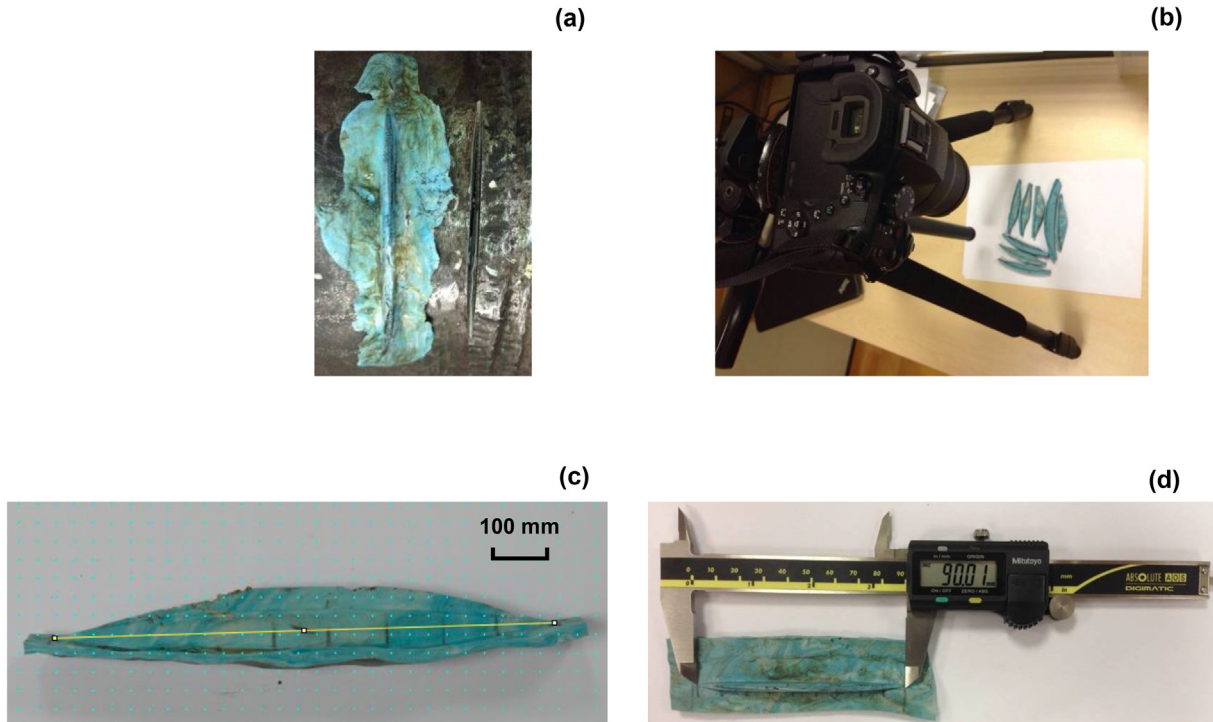


Fig. 6. Measurement of crack sizes from the replica-reproduced fracture surface: (a) reconstruction of the fracture surface using replica; (b) image capture; (c) image processing; and (d) digital caliper measurement.

To size the detected crack, Fig. 4 presents two different approaches based on the velocity of the ultrasonic shear wave in the material. Based on the angles of the emitting ultrasonic waves, α_1 and β_1 , and the horizontal distance, S_1 , between the emitting point and crack, the crack depth becomes,

$$\begin{cases} h_1 = \frac{S_1}{\tan(\alpha_1)} - \frac{S_1}{\tan(\beta_1)} \\ d_1 = \frac{S_1}{\tan(\alpha_1)} \end{cases} \quad (15)$$

where h_1 represents the height of the crack, d_1 indicates the maximum

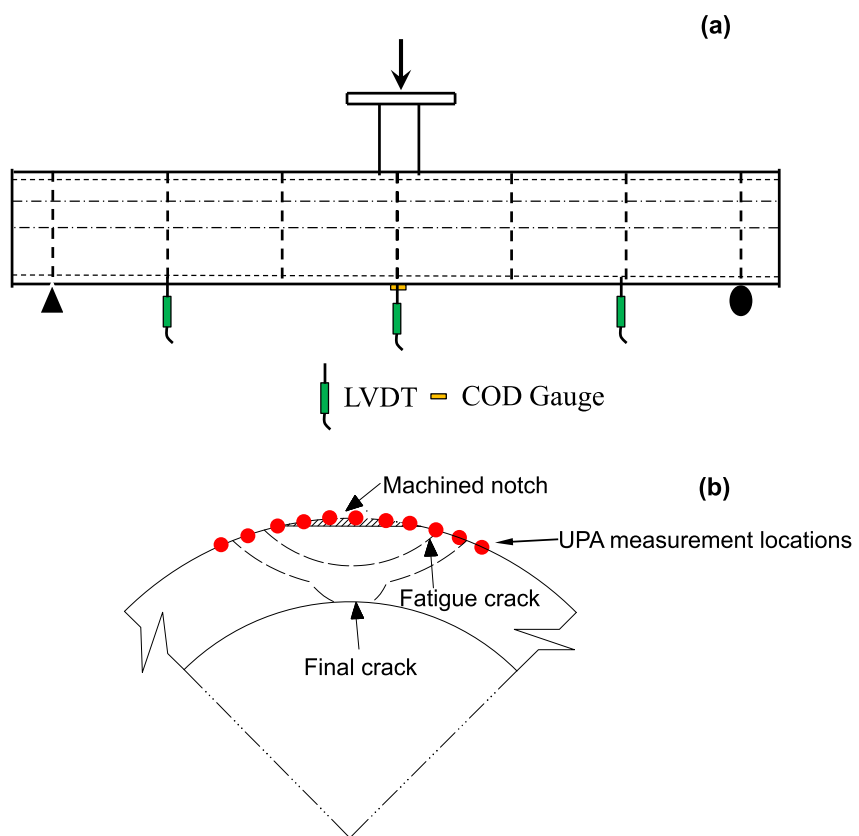


Fig. 7. (a) Experimental setup for fatigue and fracture tests for the machine-notched pipe specimens; and (b) a section view of the cracked section.

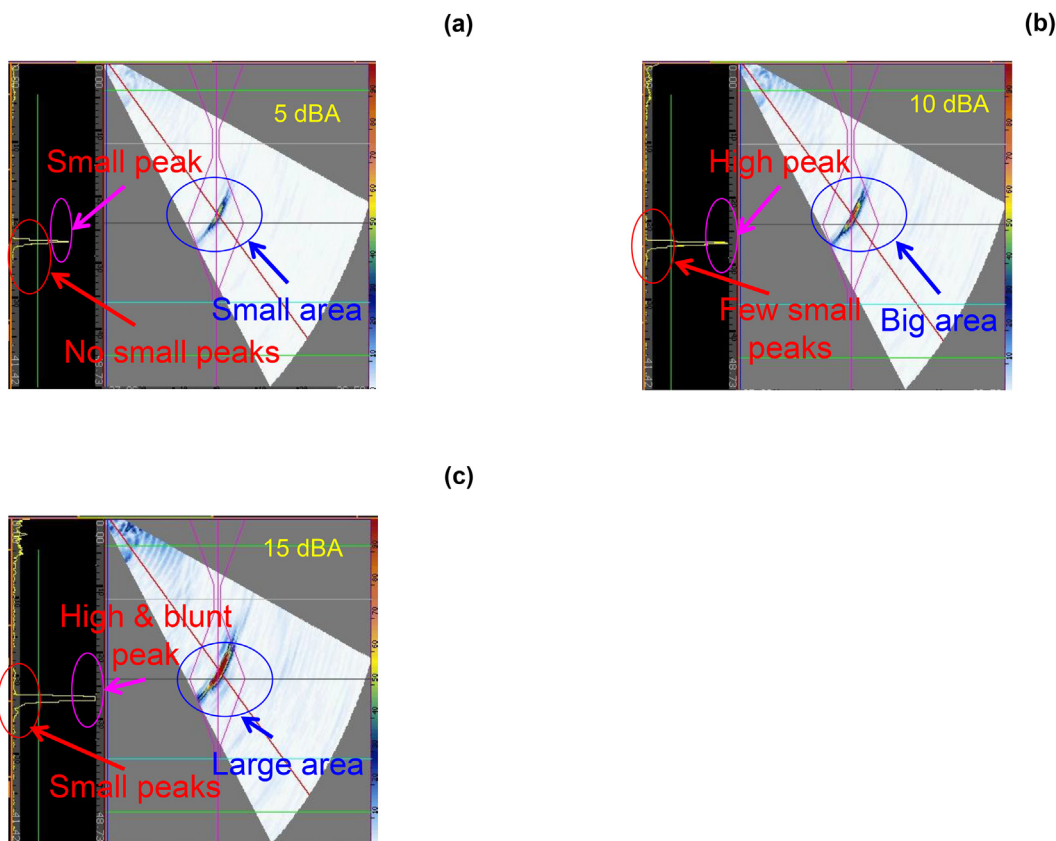


Fig. 8. UPA results comparison at different gains; (a) 5 dBA; (b) 10 dBA; and (c) 15 dBA.

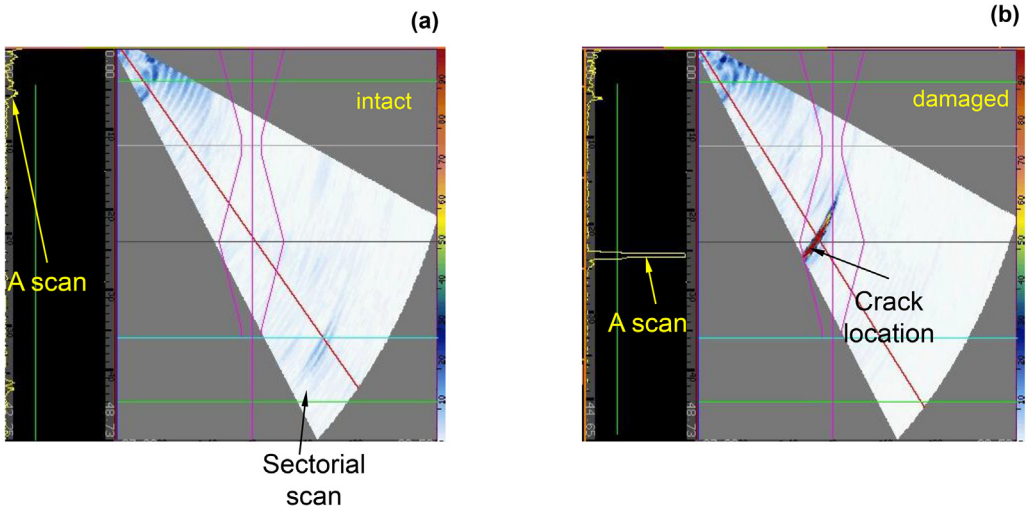


Fig. 9. Typical UPA results for: (a) intact condition; and (b) cracked condition.

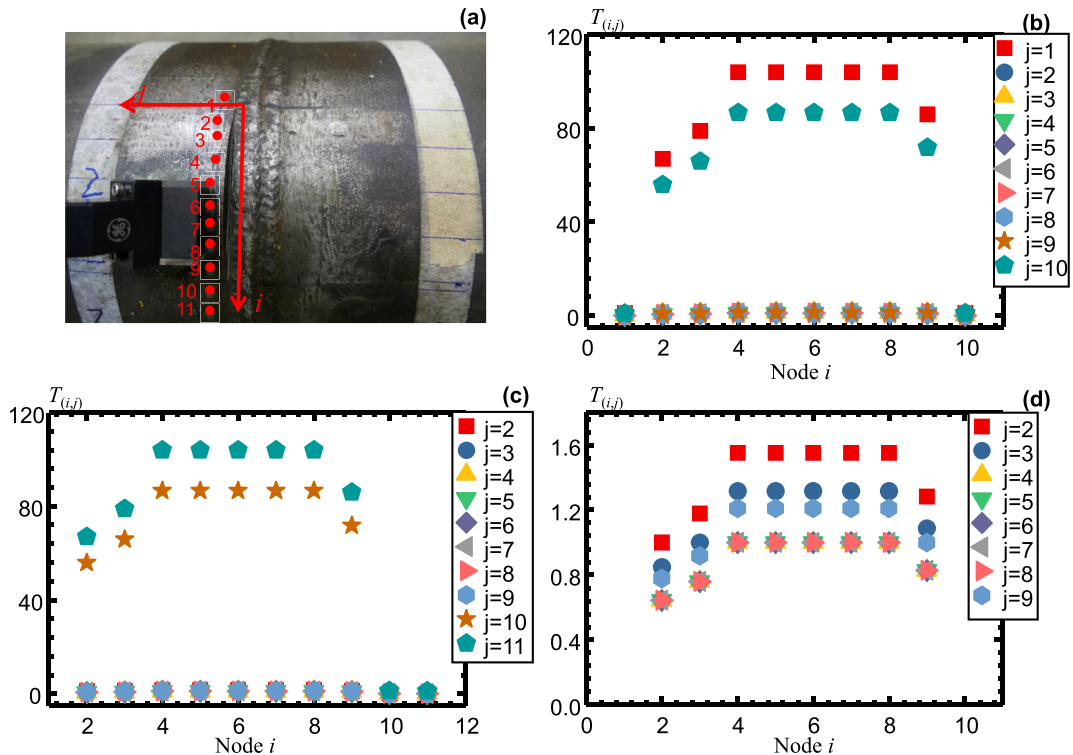


Fig. 10. Transmissibility $T_{(i,j)}$ for Pipe 2: (a) locations for the test nodes 1 to 11; (b) calculated from node 1 to 10 only; (c) calculated from node 2 to 11 only; and (d) calculated from node 2 to 9 only.

crack depth. This approach relies on the value ' S_1 ', which depends on the velocity of the ultrasonic shear wave velocity and therefore the material used. To ensure accurate crack sizing using this approach, a detailed analysis on the ultrasonic waves in the inspected material becomes necessary.

To allow for crack sizing based purely on the A-scan data, Fig. 4b illustrates an alternative approach via moving the UPA sensor by a small distance S_2 . As shown in Fig. 4b, the distances from the UPA sensors to the crack location, e.g., the crack front position, correspond to,

$$\begin{cases} SR_1 \times \cos \alpha_2 = SR_2 \times \cos \beta_2 \\ SR_1 \times \sin \alpha_2 - SR_2 \times \sin \beta_2 = S_2 \end{cases} \quad (16)$$

where SR_1 and SR_2 indicate the traveling distance of the A-scan wave

from the emitting location to the crack front, respectively. The angles α_2 and β_2 refer to the emitting angle of the A-scan wave to the crack-front position for SR_1 and SR_2 , respectively. The crack depth thus follows,

$$\begin{aligned} d_2 &= SR_1 \times \cos \alpha_2 \\ &= \frac{S_2}{(\sin \alpha_2 \times \cos \beta_2 - \cos \alpha_2 \times \sin \beta_2)} \cos \alpha_2 \times \cos \beta_2 \\ &= S_2 \times \frac{\cos \alpha_2 \times \cos \beta_2}{\sin(\alpha_2 - \beta_2)} \end{aligned} \quad (17)$$

where d_2 quantifies the crack depth. Equation (17) measures the depth of the crack-front position depending solely on the emitting angles and the horizontal movement S_2 . Calculations of d_2 based on a practical range of S_2 used in the experiment leads to an accurate estimation of the crack-front position. This study determines the individual crack-front locations through Eq. (17) along the curved surface crack front for all

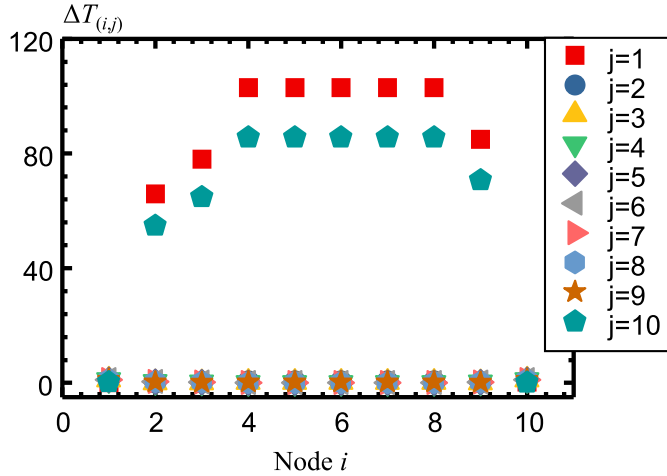


Fig. 11. The crack indicator $\Delta T_{(i,j)}$ for Pipe 2 calculated from node 1 to 10.

welded pipe specimens using $0.2t < S_2 < 0.5t$, where t is the thickness of the specimen. In Eq. (17), the angle α_2 remains larger than β_2 , which will guarantee the correct calculation of d_2 . If the UPA probe approaches the crack in measurement, the former probe location corresponds to α_2 , while the latter position corresponds to β_2 .

Compared to the conventional ultrasonic phased array approach, this study tries to apply transmissibility in A-scan data solely in crack sizing without the reference setting for calibration and material. Equation (14) determines the crack occurrence and Eq. (17) quantifies

the crack depth.

3. Conventional UPA and replica measurement

This section presents two different techniques, the conventional UPA method and the direct measurement from the replica-reproduced fracture surface, used in this study to confirm the accuracy of the proposed approach in detecting and sizing the surface cracks in the welded pipe specimens.

The UPA test measures discontinuities in the material via generating and receiving ultrasonic waves from the same array of piezoelectric elements, covering a range of refracted angles. The UPA test calculates the distance from the detected discontinuity to the ultrasonic probe by multiplying the transit time for the reflected wave at the material discontinuity and the velocity of the ultrasonic wave in the material. The UPA test often provides a series of different presentations of the measured data, including the A-scan data in the waveform display with the amplitude of the ultrasonic wave indexed against the transit time, the cross-section B-scan by plotting successive A-scan data together to reveal the scanned cross section, the sectorial scan which converts the waveform A-scan data into a colored image. The occurrence and location of the defects become clearly reflected in the sectorial scan images. Fig. 5 illustrates the typical A-scan and sectorial scan data retrieved from the UPA measurement for the surface cracks in one of the welded pipe specimens.

In addition to the conventional UPA test, this study utilizes the silica-replica to reproduce the fracture surface of the specimen. Images taken from a high-resolution camera allows direct measurement of the

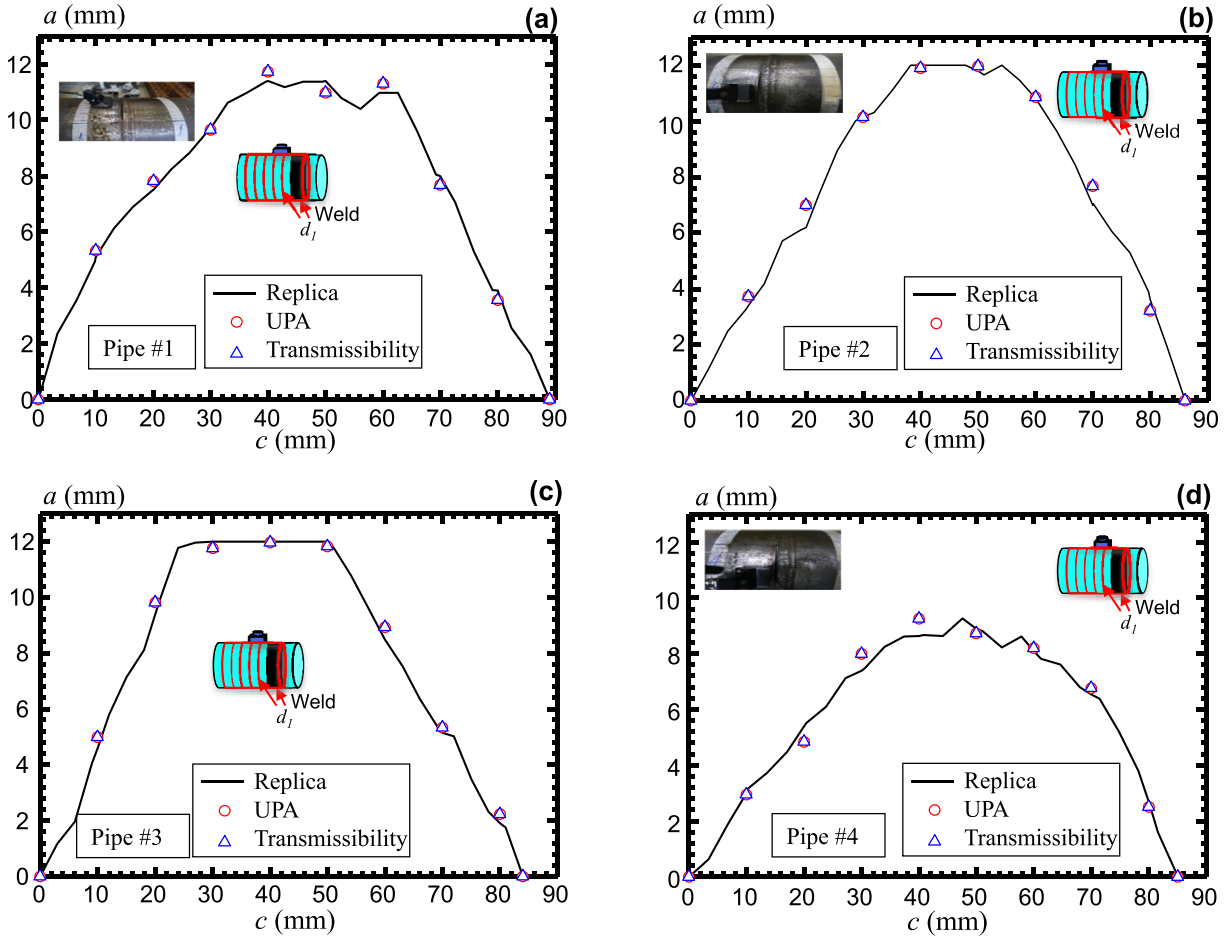


Fig. 12. Comparison of the crack size measurement using replica measurement, conventional UPA, and transmissibility-based A-scan data measurement for: (a) pipe 1; (b) pipe 2; (c) pipe 3; and (d) pipe 4.

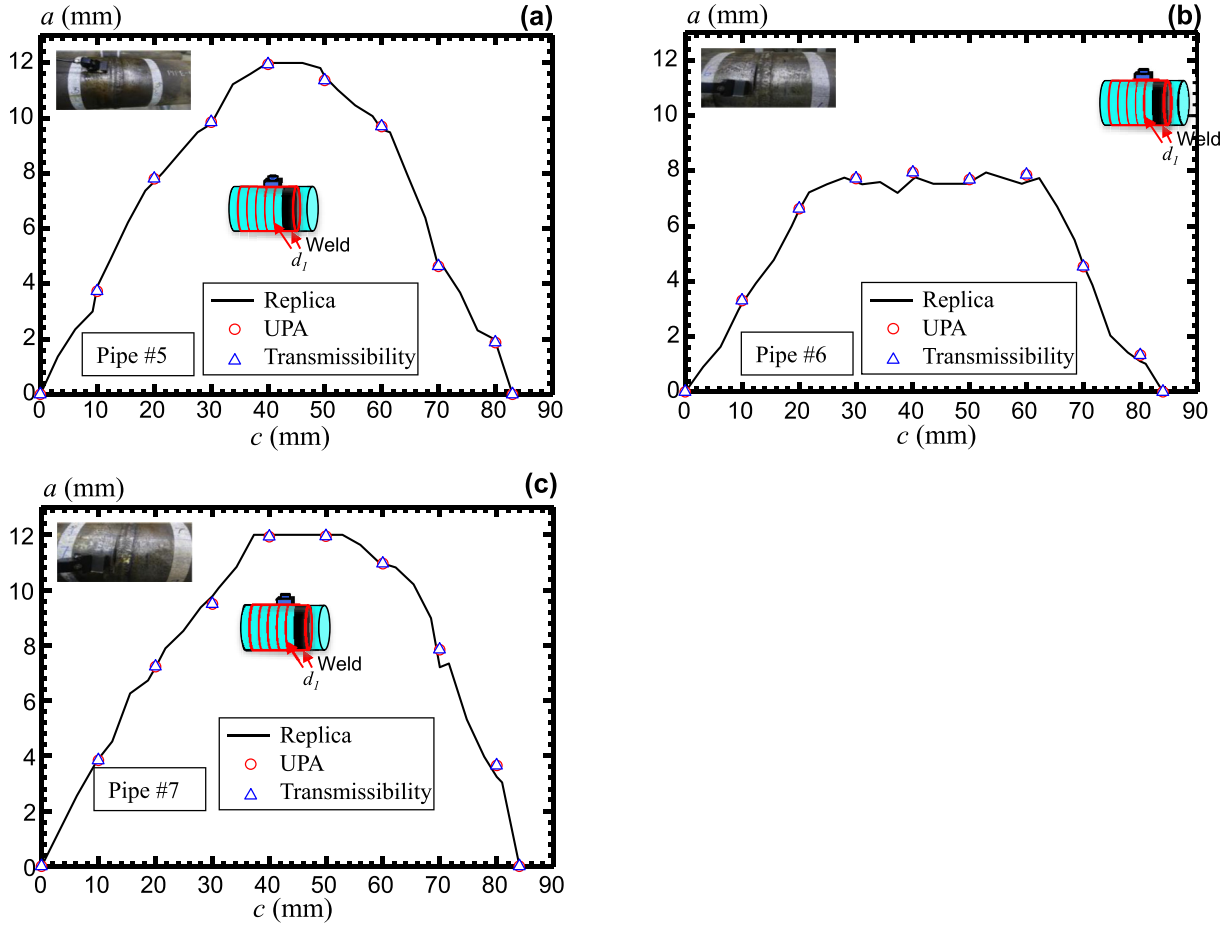


Fig. 13. Comparison of the crack size measurement using replica measurement, conventional UPA, and transmissibility-based A-scan data measurement for: (a) pipe 5; (b) pipe 6; and (c) pipe 7.

crack size along the curved crack front in the welded pipes. Direct measurement from the replica-reproduced fracture surface provides a reference to gage the accuracy of the proposed method. Fig. 6 shows the typical procedures involved in measuring the crack size from a replica-reproduced surface.

4. Experimental program

This section presents the experimental program on the welded pipes to validate the above crack detection and sizing approach. The welded pipes, fabricated from S355 steels with a machined surface notch, has previously experienced cyclic loading to generate a fatigue crack, followed by a monotonic loading to examine the fracture resistance [48].

The experimental program consists of seven surface-cracked pipe specimens tested under fatigue and fracture actions previously reported in the development of $J-R$ curve measurement directly from surface-cracked pipes [14,48]. Each test specimen consists of two straight 1-m pipes connected by circumferential girth welding. Along the toe of the girth welds locates a semi-elliptical, machined notched with 7 mm in depth (a), and 85 mm in length ($2c$). The diameter (d_0) for all the pipe specimens equals 244.5 mm, with the thickness of 12 mm and a span of 1800 mm. The numbering of the pipe specimens follows a sequential number from Pipe #1 to Pipe #7. Fig. 7 illustrates the three-point bend setup for the fatigue and fracture test. The cyclic test with a load ratio of 0.1 and a frequency of 2 Hz generates a sharp crack front along the semi-elliptical notch of the specimen. The fatigue test terminates as the maximum crack depth reaches about 70–80% of the wall thickness. During the fracture test, the deepest crack-front location penetrates through the thickness of the pipe.

Prior to the measurement, the UPA equipment undergoes a calibration to ensure its accuracy in detecting flaws for the S355 steel materials. The machine calibration of the UPA machine, Phasor XS™ Portable Phased Array Ultrasonic Flaw Detector, follows the initial setup by the manufacturer. Additional adjustment on the gain, which represents the compensation to ultrasonic signals, is necessary to optimize the performance of the UPA machine to the testing environment in the laboratory. The optimal level of the gain is a compromise between the accurate detection of large defects and the pick-up of small material discontinuities. A low level of gain allows accurate crack sizing, but may neglect small discontinuities in the material. On the other hand, a high level of compensation to the signal (a large gain) will include both the large defects and small discontinuities. However, when these small discontinuities locate very close to the large crack, the sizing of the large crack become over-estimated. Fig. 8 demonstrates the UPA measurement at the same cracked location of the welded pipe under three different gains: 5 dBA, 10 dBA, and 15 dBA. The increase in gain leads to a higher magnitude of the A-Scan data in Fig. 8. Subsequent testing reported in this study uses a standard gain level of 10 dBA. In addition to the equipment calibration, we have performed the user calibration following BS EN ISO 7963 [49] using a curved reference block.

The UPA measurement on each of the seven cracked pipes selects eleven measurement locations, as illustrated in Fig. 5b. For the test specimens, the A-scan data at materials far away from the cracked region (see Fig. 3) allows the calculation of the reference transmissibility for the undamaged material used in estimating the crack indicator in Eq. (14). This study identifies the reference locations through the collected values of transmissibility for both the damaged and undamaged material, assuming that the material damage condition is not known a

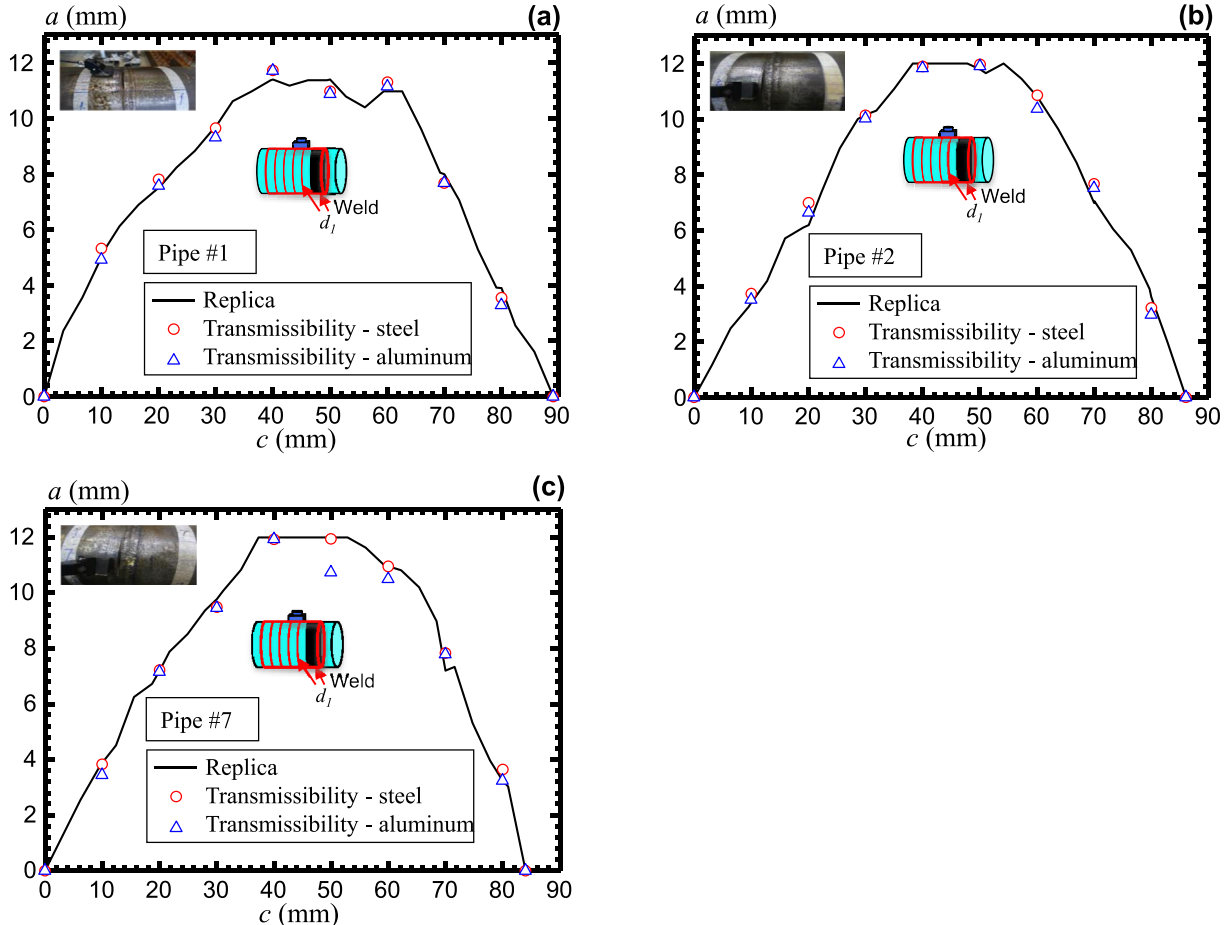


Fig. 14. Comparison of the crack size measurement using replica measurement and transmissibility-based A-scan data measurements calibrated for steel and aluminum alloy materials for: (a) pipe 1; (b) pipe 2; and (c) pipe 7.

prior. By moving the UPA probe along the toe of the girth welds at different locations, the corresponding A-scan data for each location allow the construction of the transmissibility matrix shown in Eq. (13) with the corresponding crack indicator in Eq. (14). Both the transmissibility value and the crack indicator show a clear difference in their magnitudes between intact and cracked area. This enables a straightforward approach in selecting the reference locations and their transmissibility.

5. Results and discussions

Fig. 9 compares the UPA A-scan and sectorial scan retrieved from the intact materials and that near the cracked material. In the undamaged material shown in Fig. 9a, the amplitude of the A-scan remains very low. The UPA equipment picks up the discontinuity if the amplitude of the A-scan exceeds an artificially selected cut-off value (the green line in Fig. 9a). The sectorial scan in Fig. 9a thus does not indicate any defects or discontinuities in the material. For the cracked material shown in Fig. 9b, the amplitude of the A-scan data shows a clear peak, which translates into a clear red zone in the sectorial scan. The UPA measurement determines the location of the discontinuity using the software integrated with the UPA equipment. The transmissibility-enhanced UPA determines the depth of the discontinuity from Eq. (17).

5.1. Transmissibility-based crack detection

For the transmissibility-based crack detection, establishment of a reference condition remains the key. Fig. 10 shows the values of

transmissibility, which equals the ratio of the peak amplitude of A-scan data measured at location i with respect to that at location j , for the welded Pipe #2. The $T_{(i,j)}$ value corresponding to a fixed position i in horizontal axis represents the ratio of the peak A-scan amplitude at i over the other locations at j , from node 1 to 10, from node 2 to 11, and from node 2 to 9, respectively. In Fig. 10b, two clear fluctuations in the $T_{(i,j)}$ values exist between reference node 1 and node 2, and between node 9 and node 10. The large $T_{(i,j)}$ values from nodes 2 to 9, referenced to the peak A-scan amplitude at nodes 1 and 10, imply that these nodal positions correspond to the damaged locations. The very small $T_{(i,j)}$ values at nodes 1 and 10 with reference to all other nodes indicate that these two positions remain intact. In order to confirm the detected damaged locations in Figs. 10b and c illustrate the transmissibility evaluation for a separate set of the locations for the same pipe, i.e., nodes 2 to 11. The high values $T_{(i,j)}$ for nodes 2 to 9, referenced to the peak amplitudes at node 10 and 11, re-affirms the damaged locations from nodes 2 to 9. The low $T_{(i,j)}$ values of nodes 10 and 11, referenced to all other nodes, suggest that the corresponding positions remain intact. Figs. 10b and c show that the $T_{(i,j)}$ values, when referenced with respect to the peak A-scan amplitude of the damaged location, remains relatively low. Fig. 10d illustrates a scenario when all sampled locations for the UPA detection correspond to the damaged locations. The $T_{(i,j)}$ values shown in Fig. 10d includes only the nodes 2 to 9. The magnitude of the $T_{(i,j)}$ values remain relatively low, without steep fluctuations among the individual nodes. This implies that all selected locations are either intact or damaged. For the transmissibility-based detection to be effective, the UPA A-scan data should cover both the intact and damaged materials. Fig. 11 illustrates the crack sensitive indicator $\Delta T_{(i,j)}$ for Pipe #2, which confirms the conclusion derived from Figs. 10b and c.

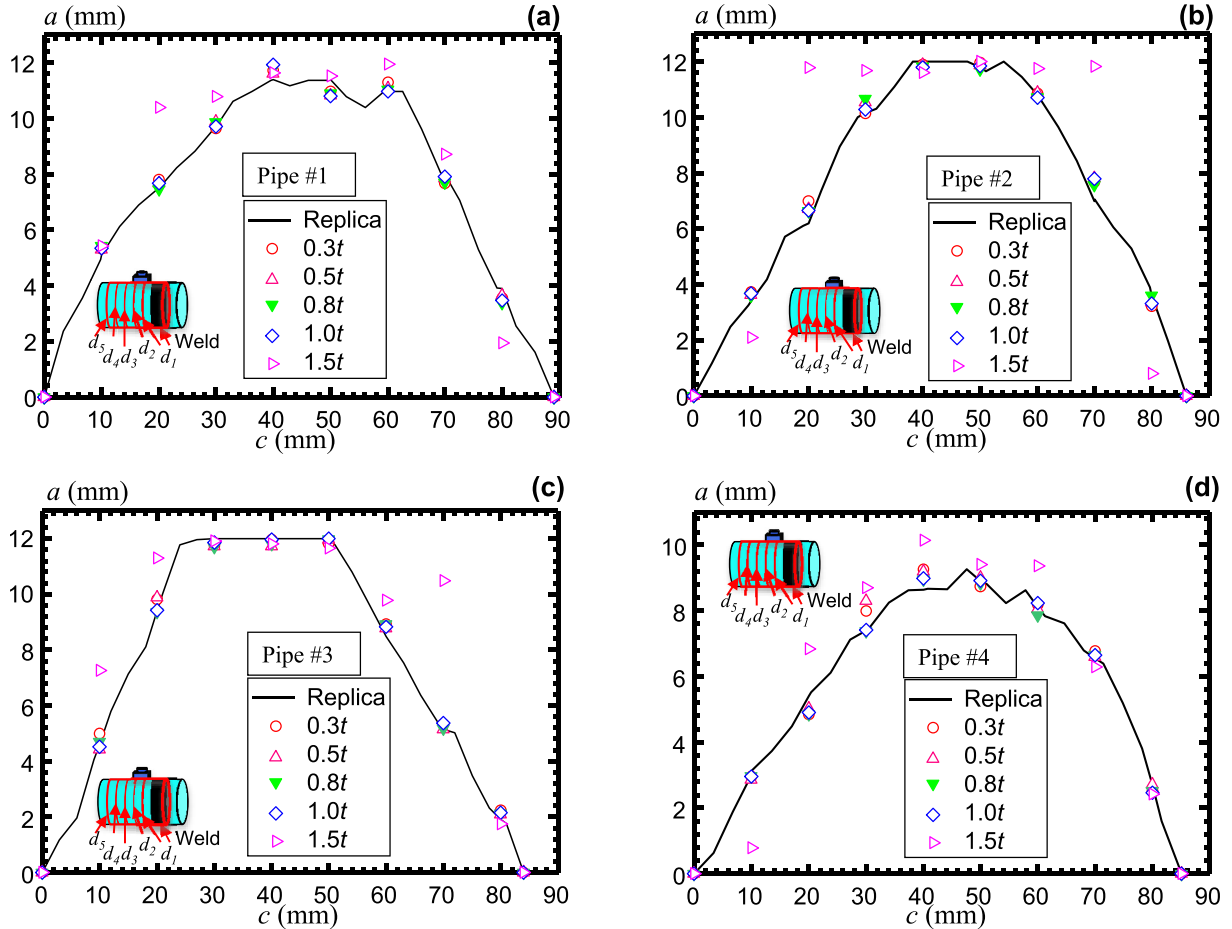


Fig. 15. Effect of UPA probe location on the measured crack size for: (a) pipe 1; (b) pipe 2; (c) pipe 3; and (d) pipe 4.

5.2. Crack sizing

Figs. 12 and 13 compare the crack sizes measured for all seven pipe specimens using the replica-reproduced fracture surface, the conventional UPA approach and the transmissibility based A-scan data (Eq. (17)), respectively. The UPA measurement shown in Figs. 12 and 13 correspond to the UPA prior calibrated against a reference block fabricated from the S355 steel. The results in Figs. 12 and 13 confirm the accuracy of the transmissibility-based approach.

5.3. Transmissibility-based approach without calibration

The fundamental theory of transmissibility implies that the calibration of the UPA data becomes non-essential, as the crack detection depends solely on the ratio of the peak magnitudes of A-scan data measured at different locations. The calculation of the crack size in Eq. (17) also remains independent of the user-calibration procedure. To examine the transmissibility-based measurement on the calibration block, this section compares the transmissibility-based crack size measurement against two different calibration blocks, the S355 steel and an aluminum alloy. In the steel material, the longitudinal wave has a velocity of 5700 m/s, and the shear wave velocity equals 3200 m/s. In the aluminum alloy, however, the longitudinal wave velocity is equal to 6299 m/s, and the shear wave velocity is 3100 m/s.

Fig. 14 compares the crack size measured by the transmissibility-based approach using two different calibration materials for three selected pipes, Pipe #1, #2 and #7, respectively. The results in Fig. 14 confirm that the transmissibility-based crack size measurement agrees closely with the direct measurement on the replica-reproduced fracture surface, independent of the calibration material used.

5.4. Sensitivity to the probe-to-crack distance

This sub-section examines the effect of the distance between the UPA probe and the crack location on the crack sizing accuracy. The experimental measurement includes five different distances between the UPA probe and the crack, 0.3t, 0.5t, 0.8t, 1.0t and 1.5t, where t represents the thickness of the welded pipe. Figs. 15 and 16 compare the crack sizes measured using the transmissibility-based approach using the A-scan data measured at these five different locations. The crack sizes measured at 1.5t indicate a high level of inaccuracy, while all measurements with the distance between the probe and crack location below 1.0t matches closely the direct measurement from the replica-reproduced fracture surface. The quality of the decoding for the ultrasonic signals in the current UPA equipment decays rapidly once the UPA probe locates more than 1t distance away from the cracked location.

6. Summary and conclusions

This study proposes a transmissibility-based treatment on the UPA A-scan data to identify and size the surface cracks in pipes with circumferential welds. The transmissibility for the A-scan data refers to the ratio of the peak amplitude of the A-scan at a location over that of another. The transmissibility-based approach entails the following advantages, which: 1) allow a convenient detection of the damaged locations for a sufficiently large number of UPA detection samples, covering both the intact and the cracked positions; and 2) do not rely on the type of the reference material in identifying and sizing the flaw. This study reports an experimental study to validate the proposed transmissibility-based approach and supports the following

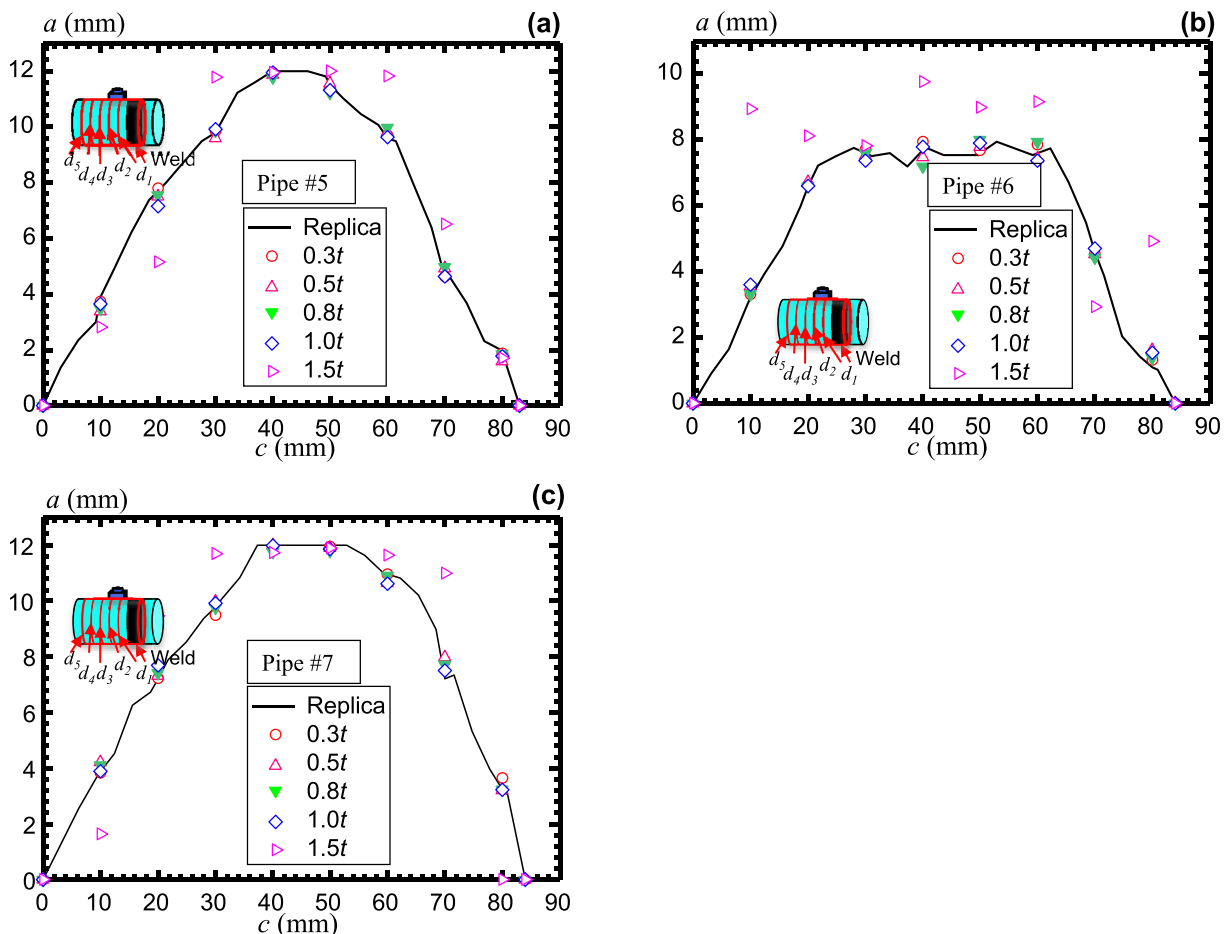


Fig. 16. Effect of UPA probe location on the measured crack size for: (a) pipe 5; (b) pipe 6; and (c) pipe 7.

conclusions:

- 1) The transmissibility treatment of the UPA A-scan data identifies and sizes the surface crack near the toe of the girth welds in pipes. The identified crack size agrees closely with those measured using the conventional, calibrated UPA and directly from the replica-reproduced fracture surface.
- 2) The detection and sizing of the surface cracks remain independent of the reference block used in the UPA calibration. The crack size identified by the transmissibility-treated A-scan data using the calibrated UPA signal for both the steel material and aluminum material agree well with the crack size measured from the replica-reproduced fracture surface.
- 3) For a sufficiently accurate measurement of the crack size, the distance between the UPA probe and the crack location should be within a $1t$ distance, where t denotes the wall thickness of the pipe, due to the quality of decoding in the current UPA equipment.

Acknowledgment

The authors would like to acknowledge the financial contribution provided by the Singapore Maritime Institute (SMI) (SMI-2015-OF-06), as well as the supports provided by American Bureau of Shipping, Eddyfi Europe SAS, and Ashtead Technology Pte Ltd.

Appendix A. Supplementary data

Supplementary data related to this article can be found at <https://doi.org/10.1016/j.ijpvp.2018.09.006>.

References

- [1] J. Ni, M.A. Wahab, A numerical kinematic model of welding process for low carbon steels, *Comput. Struct.* 186 (2017) 35–49.
- [2] J. Ni, X. Wang, J. Gong, M.A. Wahab, Thermal, metallurgical and mechanical analysis of circumferentially multipass welded P92 steel pipes, *Int. J. Pres. Ves. Pip.* 165 (2018) 164–175.
- [3] J. Ni, J.V. Voorde, J. Antonissen, M.A. Wahab, Dependency of phase transformation on the prior austenite grain size and its influence on welding residual stress of S700 steel, *Weld. World* 62 (2018) 699–712.
- [4] S. Datta, S. Sarkar, A review on different pipeline fault detection methods, *J. Loss Prevent. Proc.* 41 (2016) 97–106.
- [5] X. Qian, K. Jitpairrod, P.W. Marshal, S. Swaddiwudhipong, Z. Ou, Y. Zhang, M.R. Pradana, Fatigue and residual strength of concrete-filled tubular X-joints with full capacity welds, *J. Constr. Steel Res.* 100 (2014) 21–35.
- [6] S.P. Chiew, S.T. Lie, C.K. Lee, Z.W. Huang, Fatigue performance of cracked tubular T joints under combined loads. I: experimental, *J. Struct. Eng. ASCE* 130 (2004) 562–571.
- [7] X. Qian, Z. Ou, S. Swaddiwudhipong, P.W. Marshal, Brittle failure caused by lamellar splitting in a large-scale tubular joint with fatigue cracks, *Mar. Struct.* 34 (2013) 185–204.
- [8] R. Tessier, R.W. Coade, B. Geneve, Sizing of cracks using the alternating current field measurement technique, *Int. J. Pres. Ves.* 79 (2002) 549–554.
- [9] C. Einnaceur, A. Laksimi, C. Herve, M. Cherfaour, Monitoring crack growth in pressure vessel steels by the acoustic emission technique and the method of potential difference, *Int. J. Pres. Ves.* 83 (2006) 197–204.
- [10] Y. Sato, T. Atsumi, T. Shoji, Continuous monitoring of back wall stress corrosion cracking growth in sensitized type 304 stainless steel weldment by means of potential drop techniques, *Int. J. Pres. Ves.* 84 (2007) 274–283.
- [11] M.G. Droubi, N.H. Faisal, F. Orr, J.A. Steel, M. El-Shaib, Acoustic emission method for defect detection and identification in carbon steel welded joints, *J. Constr. Steel Res.* 134 (2017) 28–37.
- [12] X.D. Liu, D.H. Xiao, Y.C. Shan, Q. Pan, T. He, Y. Gao, Solder joint failure localization of welded joint based on acoustic emission beamforming, *Ultrasonics* 74 (2017) 221–232.
- [13] I.A. Khan, P. Ahuja, S. Satpute, M.A. Khan, V. Bhaisin, K.K. Vaze, A.K. Ghosh, M. Saravanan, S. Vishnuvardhan, D.M. Pukazhendi, P. Gandhi, G. Raghava, Fracture investigations on piping system having large through-wall circumferential

- crack, Int. J. Pres. Ves. Pip. 88 (2011) 223–230.
- [14] N. Parool, X. Qian, C.G. Koh, An η -compliance method to estimate the $J\Delta$ curve for pipes with a circumferential surface crack, Fatig. Fract. Eng. Mater. Struct. 40 (2017) 1624–1639.
- [15] X. Qian, Y. Li, A compliance based approach to measure fracture resistance curve for surface-cracked plates, Int. J. Fract. 182 (2013) 1–19.
- [16] A. Bouloudenine, M. Feliachi, M.E. Latreche, Development of circular arrayed eddy current sensor for detecting fibers orientation and in-plane fiber waviness in unidirectional CFRP, NDT Int. 92 (2017) 30–37.
- [17] O. Karpenko, C.F. Ye, L. Udupa, Dual frequency fusion for defect signal enhancement in EC-GMR inspection of riveted multilayer structures, NDT Int. 92 (2017) 97–103.
- [18] Y. Ohara, T. Oshiumi, H. Nakajima, K. Yamanaka, X. Wu, T. Uchimoto, T. Takagi, T. Tsuji, Miura, Ultrasonic phased array with surface acoustic wave for imaging cracks, AIP Adv. 7 (2017) 065214.
- [19] S.O. Pilyugin, V.P. Lunin, Determining the probability of detecting flaws in weld joints by phased-array ultrasonic testing, Russ. J. Nondestruct. + 52 (2016) 332–338.
- [20] B.W. Drinkwater, P.D. Wilcox, Ultrasonic arrays for non-destructive evaluation: a review, NDT Int. 39 (2016) 525–541.
- [21] Schmerr LWJr, Fundamentals of Ultrasonic Phased Arrays, Springer International Publishing Switzerland, 978-3-319-07271-5, 2015, <https://doi.org/10.1007/978-3-319-07272-2>.
- [22] Y.L. Zhou, N.M.M. Maia, M.A. Wahab, Damage detection using transmissibility compressed by principal component analysis enhanced with distance measure, J. Vib. Contr. (2017), <https://doi.org/10.1177/1077546316674544>.
- [23] P. Razi, F. Taheri, A vibration-based strategy for health monitoring of offshore pipelines' girth-welds, Sensors 14 (2014) 17174–17191.
- [24] Z.-G. Jia, L. Ren, H.-N. Li, S.-C. Ho, G.-B. Song, Experimental study of pipeline leak detection based on hoop strain measurement, Struct. Control Hlth. 22 (2015) 799–812.
- [25] M. Dilena, M.F. Dell'Oste, A. Morassi, Detecting cracks in pipes filled with fluid from changes in natural frequencies, Mech. Syst. Signal Process. 25 (2011) 3186–3197.
- [26] M.G. Lozev, R.L. Spencer, D. Hodgkinson, Optimized inspection of thin-walled pipe welds using advanced ultrasonic techniques, J. Press Vess-T ASME 127 (2005) 237–243.
- [27] M. Moles, N. Dubé, S. Labbé, E. Ginzel, Review of ultrasonic phased arrays for pressure vessel and pipeline weld inspections, J. Press Vess-T ASME 127 (2005) 351–356.
- [28] D.J. Huggett, M.W. Dewan, M.A. Wahab, A. Okeil, T.W. Liao, Phased array ultrasonic testing for post-weld and OnLine detection of friction stir welding defects, Res. Nondestr. Eval. 28 (2017) 187–210.
- [29] N. Oiwa, K. Kida, T. Iwaki, T. Okada, T. Ishikawa, N. Eguchi, K. Nanba, A test of phased array ultrasonic testing of aluminium alloy friction stir welded joints, Weld. Int. 22 (2008) 511–517.
- [30] S. Alavudeen, C.V. Krishnamurthy, K. Balasubramaniam, D.M. Pugazhendhi, G. Raghava, P. Gandhi, Improved imaging of fatigue crack profile in thick cruciform samples using ultrasonic phased array models, J. Press Vess-T ASME 132 (2010) 011501.
- [31] S. Yang, B. Yoon, Y. Kim, Using phased array ultrasonic technique for the inspection of straddle mount-type low-pressure turbine disc, NDT Int. 42 (2009) 128–132.
- [32] Z. Bai, S. Chen, L. Jia, Z. Zeng, Phased array ultrasonic signal compressive detection in low-pressure turbine disc, NDT Int. 89 (2017) 1–13.
- [33] A. Leleux, P. Micheau, M. Castaings, Long range detection of defects in composite plates using lamb waves generated and detected by ultrasonic phased array probes, J. Nondestr. Eval. 32 (2013) 200–214.
- [34] N. Xu, Z. Zhou, Numerical simulation and experiment for inspection of corner-shaped components using ultrasonic phased array, NDT Int. 63 (2014) 28–34.
- [35] D. Duxbury, J. Russell, M. Lowe, The effect of variation in phased array element performance for non-destructive evaluation (NDE), Ultrasonics 53 (2013) 1065–1078.
- [36] P.D. Wilcox, C. Holmes, Drinkwater BW advanced reflector characterization with ultrasonic phased arrays in NDE applications, IEEE T Ultrason Ferr. 54 (2007) 1541–1550.
- [37] X. Guan, J. Zhang, S.K. Zhou, E.M. Rasselkorde, W.A. Abbasi, Post-processing of phased-array ultrasonic inspection data with parallel computing for nondestructive evaluation, J. Nondestr. Eval. 33 (2014) 342–351.
- [38] Y.L. Zhou, E. Figueiredo, N.M.M. Maia, R. Sampaio, R. Perera, Damage detection in structures using a transmissibility-based mahalanobis distance, Struct. Control Hlth. 22 (2015) 1209–1222.
- [39] Y.L. Zhou, E. Figueiredo, N.M.M. Maia, R. Perera, Damage detection and quantification using transmissibility coherence analysis, Shock Vib. (2015) 290714.
- [40] Y.L. Zhou, H. Cao, Q. Liu, M.A. Wahab, Output based structural damage detection by correlation analysis together with transmissibility, Materials 10 (2017) 866 1–86617.
- [41] Y.L. Zhou, N.M.M. Maia, R. Sampaio, M.A. Wahab, Structural damage detection using transmissibility together with hierarchical clustering analysis and similarity measure, Struct. Health Monit. 16 (2017) 711–731.
- [42] Y.L. Zhou, M.A. Wahab, Cosine based extended transmissibility damage indicators for structural damage detection, Eng. Struct. 141 (2017) 175–183.
- [43] Y.L. Zhou, Structural Health Monitoring by Using Transmissibility, PhD thesis Technical University of Madrid, Spain, 2015.
- [44] S. Carcangiu, A. Montisci, R. Forciniti (Eds.), Numerical Simulation of Wave Propagation. Ultrasonic Nondestructive Evaluation Systems Industrial Application Issues, Springer Cham Heidelberg NewYork Dordrecht London, Springer International Publishing Switzerland, 978-3-319-10565-9, 2015, , <https://doi.org/10.1007/978-3-319-10566-6>.
- [45] P.L. Arlett, A.K. Bahrani, O.C. Zienkiewicz, Application of finite elements to the solution of Helmholtz's equation, Proc. IEEE 115 (1968) 1762–1766.
- [46] I. Harari, A survey of finite element methods for time-harmonic acoustics, Comput. Meth. Appl. Mech. Eng. 195 (2006) 1594–1607.
- [47] D.J. Ewins, MODAL TESTING: Theory, Practice and Application (Mechanical Engineering Research Studies: Engineering Dynamics Series), second ed., Mechanical Engineering Research, 2009 ISBN-10: 0863802184, ISBN-13: 978-0863802188.
- [48] N. Parool, X. Qian, C.G. Koh, A modified hybrid method to estimate fracture resistance curve for pipes with a circumferential surface crack, Eng. Fract. Mech. 188 (2018) 1–19, <https://doi.org/10.1016/j.englfracmech.2017.05.046>.
- [49] BS EN ISO, 7963. Non-destructive Testing—Ultrasonic Testing —Specification for Calibration Block No. 2, (2010).